European Journal of Medicinal Chemistry 256 (2023) 115446

Contents lists available at ScienceDirect

European Journal of Medicinal Chemistry

journal homepage: www.elsevier.com/locate/ejmech

Research paper

A cyanine-based NIR fluorescent Vemurafenib analog to probe BRAF^{V600E} in cancer cells

Elisabetta Barresi [a,b], Caterina Baldanzi [c,d], Marta Roncetti [c,d,e], Michele Roggia [g], Emma Baglini [a], Irene Lepori [c,d,f], Marianna Vitiello [c,d], Silvia Salerno [a,b], Lorena Tedeschi [c], Federico Da Settimo [a,b], Sandro Cosconati [g], Laura Poliseno [c,d,**], Sabrina Taliani [a,b,*]

[a] Department of Pharmacy, University of Pisa, Via Bonanno 6, 56126, Pisa, Italy
[b] Center for Instrument Sharing of the University of Pisa (CISUP), University of Pisa, Lungarno Pacinotti 43/44, 56126, Pisa, Italy
[c] Institute of Clinical Physiology, CNR, Via Moruzzi 1, 56124, Pisa, Italy
[d] Oncogenomics Unit, Core Research Laboratory, ISPRO, Via Moruzzi 1, 56124, Pisa, Italy
[e] University of Siena, Siena, Italy
[f] Department of Microbiology, University of Massachusetts, Amherst, MA, USA
[g] DiSTABiF, University of Campania "Luigi Vanvitelli", Via Vivaldi 43, 81100, Caserta, Italy

ARTICLE INFO

Keywords:
BRAF^{V600E}
Vemurafenib
Melanoma
Hairy cell leukemia
Fluorescent probe
Cyanine-5

ABSTRACT

BRAF represents one of the most frequently mutated protein kinase genes and BRAF^{V600E} mutation may be found in many types of cancer, including hairy cell leukemia (HCL), anaplastic thyroid cancer (ATC), colorectal cancer and melanoma. Herein, a fluorescent probe, based on the structure of the highly specific BRAF^{V600E} inhibitor Vemurafenib (Vem, **1**) and featuring the NIR fluorophore cyanine-5 (Cy5), was straightforwardly synthesized and characterized (Vem-L-Cy5, **3**), showing promising spectroscopic properties. Biological validation in BRAF^{V600E}-mutated cancer cells evidenced the ability of **3** to penetrate inside the cells, specifically binding to its elective target BRAF^{V600E} with high affinity, and inhibiting MEK phosphorylation and cell growth with a potency comparable to that of native Vem **1**. Taken together, these data highlight Vem-L-Cy5 **3** as a useful tool to probe BRAF^{V600E} mutation in cancer cells, and suitable to acquire precious insights for future developments of more informed BRAF inhibitors-centered therapeutic strategies.

1. Introduction

Molecular targeted therapy has demonstrated remarkable clinical success in the treatment of numerous cancer types (i.e. leukemia, breast, colorectal, lung, melanoma, ovarian and thyroid cancers); the main advantage with respect to conventional chemotherapy is represented by a higher selectivity for cancer cells, with consequent lower toxicity to healthy tissues [1,2]. In this respect, the identification of ideal targets that can distinguish cancer cells from healthy cells represents an essential step. Potential cancer markers include growth and pro-angiogenesis factors, cell-cycle proteins, and modulators of apoptosis [1–4]. In turn, investigations on the physiology of these specific molecular targets in cancer are mandatory for the development of new effective strategies to host tumor growth and progression, with reduced damage on healthy cells.

Kinases play a crucial role in modulating signaling pathways involved in several processes such as cell survival, migration, and angiogenesis [5]. Overexpression or mutation of such kinases may determine aberrant cancer cell growth and propagation. Indeed, many kinase inhibitors (KIs), designed to target upregulated/mutated specific tumor cell pathways, are clinically approved to treat cancer [6]. The BRAF gene was identified in 2002 as a driver oncogene and represents one of the most frequently mutated protein kinase genes in human tumors [7]. The BRAF protein is a member of the serine threonine Raf family kinases; these are part of the Ras/RAF/MEK/ERK mitogen activated protein kinase (MAPK) signal transduction cascade that controls cell proliferation and survival [7]. The most common mutation, which accounts for about 90% of all BRAF mutations, is the valine replacement with glutamic acid at position 600 (V600E) within the kinase domain, encoding for a BRAF protein that remains constitutively activated with

* Corresponding author. Department of Pharmacy, University of Pisa, Via Bonanno 6, 56126, Pisa, Italy.
** Corresponding author. Oncogenomics Unit, Core Research Laboratory, ISPRO; Institute of Clinical Physiology (IFC), CNR, Via Moruzzi 1, 56124, Pisa, Italy.
E-mail addresses: laura.poliseno@cnr.it, l.poliseno@ispro.toscana.it (L. Poliseno), sabrina.taliani@unipi.it (S. Taliani).

https://doi.org/10.1016/j.ejmech.2023.115446
Received 11 November 2022; Received in revised form 28 April 2023; Accepted 2 May 2023
Available online 7 May 2023

an 800-fold increased kinase activity with respect to its wild-type counterpart, resulting in an uncontrolled cell proliferation [7]. $BRAF^{V600E}$ mutation has been observed in a number of severe human malignancies, including hairy cell leukemia (HCL), a relatively rare chronic B-cell malignancy [8,9], melanoma [10], as well as thyroid, and colorectal cancers [7].

As prototype of selective BRAF inhibitors (BRAFi), Vemurafenib (**1**, Vem, PLX4032, Plexxikon/Roche, Chart 1) is an ATP-competitive small molecule inhibitor. It shows selectivity for the $BRAF^{V600E}$ mutant form, reducing MEK phosphorylation, activation of the MAPK pathway and, in turn, cell proliferation [11]. It is clinically approved for the treatment of metastatic and non-resectable melanoma that harbors the $BRAF^{V600E}$ mutation [11]. In addition, Vem **1** shows noteworthy clinical activity in HCL patients [12–15]. In clinical trials involving patients with refractory or relapsed HCL, the targeting of $BRAF^{V600E}$ with Vem **1**, orally administered, led to a response in 91% of the patients, and 35% of the patients had a complete response. In spite of its efficacy, Vem **1** fails in the establishment of a durable and reproducible response unless administered at relatively high doses, and shows predisposition to acquired resistance [16,17]. The therapeutic protocol, consisting in the combination of BRAFi with MEK inhibitors, represents an improvement with respect to the BRAFi monotherapy in terms of side effects, duration of response and survival [18]. However, it does not overcome all the drawbacks described above [19]. A considerable number of advanced clinical trials are currently ongoing evaluating Vem **1** for the therapeutic treatment of several tumors including HCL, pancreatic, colorectal, thyroid and lung cancers, lymphomas, and gliomas (see https://clinicaltrials.gov/). Consequently, there is great interest in a more detailed understanding of the molecular mechanism of Vem **1** to develop a new generation of molecules able to target $BRAF^{V600E}$ more efficiently in tumors.

In this respect, fluorescent derivatives of kinase inhibitors represent useful tools for imaging studies at the cellular and sub-cellular level, aimed at investigating crucial aspects correlated to drug action, such as target selectivity, kinetics, drug exposure, the occurrence of resistance mechanisms, and pharmacodynamic effects [20]. Near-infrared (NIR, 650–900 nm) fluorophores find wide application in fundamental biological studies due to several advantages, including the correlated low energetic radiation, deep tissue penetration, and the property to minimize the interfering background deriving from autofluorescence of biomolecules [20]. Thus, the development of NIR probes constitutes a promising area of research for in vitro, in cells and in vivo imaging studies [21].

In the present paper the arsenal of imaging tools useful for the investigation on $BRAF^{V600E}$ tumors was enriched by the synthesis and chemical-physical as well as biological validation of the fluorescent probe **3** (Vem-L-Cy5, Chart 1), which is based on the structure of Vem **1** (Chart 1), and features the NIR fluorophore Cyanine-5 (Cy5, Chart 1) [21].

Of note, a further relevant result of the present project is represented by the setting-up and the optimization of a new efficient, high yield and reliable synthetic protocol for the obtainment of Vem-NH_2 **2** (Chart 1), an analog of Vem **1** bearing an amino group in place of the chlorine at the *para* position of the pendant phenyl ring, which has the potential to be easily functionalized for the conjugation with a chromophore. Indeed, compound **2** represents a useful building block for the obtainment of various molecular tools for specific application in imaging investigations on $BRAF^{V600E}$.

2. Results and discussion

2.1. Design and synthesis of Vem-L-Cy5 3

The design of probe **3** (Chart 1) takes advantage of the study by Mikula et al. [22] in which the authors developed fluorescent analogs of Vem **1** characterized by BODIPY, MayaFluor and SiRc chromophores [22]. Co-crystallization studies clarified the mode of binding of **1** with the $BRAF^{V600E}$ protein [11], and suggested the *p*-chlorophenyl substituent of **1**, pointing away from the kinase binding pocket, as the position suitable for chemical modifications. This position can be exploited for the introduction of a functional linker bound to the chromophore, without compromising the interaction with the target. Along this line, Vem-NH_2 **2** (Chart 1), in which the basic structure of **1** was modified introducing an amino group in place of the chlorine at the *para*-position of the pendant phenyl ring, was identified as the analog of Vem **1** suitable for the conjugation with the chromophore by a short polyethylene glycol (PEG)-based linker.

Based on these considerations, Vem-NH_2 **2** constitutes a key intermediate for the preparation of the probe **3** (Chart 1). Initially, we carried out the synthesis of Vem-NH_2 **2** faithfully following the experimental protocol reported by Mikula and coworkers [22]. Briefly, the described procedure involved the preparation of the bromo-intermediate **8** starting from 2,4-difluoroaniline that was reacted with 1-propanesulfonylchloride to give the corresponding sulfonamide, and then formylated at 3-position by treatment with lithium diisopropylamide and *N*-methylmorpholine; the subsequent reaction with 5-bromoazaindole in the presence of K_2CO_3 followed by DDQ-mediated oxidation should have furnished derivative **8** [22]. Surprisingly, several difficulties emerged in reproducing this synthetic pathway, especially in the formylation step [22], which compromised the whole protocol.

Thus, in the present study, a new, more reproducible, straightforward and high yield experimental procedure was set up to overcome the formylation reaction reported by Mikula et al. [22] in the preparation of the intermediate **8**, as outlined in Scheme 1. After activation with oxalyl chloride, the 2,6-difluoro-3-nitrobenzoic acid **5** is reacted with 5-bromo-7-azaindole under Friedel-Crafts conditions to furnish **6**. Reduction of the nitro group and subsequent substitution on the amino group with 1-propanesulfonylchloride give the desired sulfonamide **8**, which is reacted with 4-(*N*-Boc-amino)phenylboronic acid in the presence of Pd(ddpf)Cl_2 and then treated with trifluoroacetic acid leading to Vem-NH_2 **2**. Optimization of the experimental conditions for each step allowed to obtain the crucial intermediate Vem-NH_2 **2** with very good yields (Scheme 1). Furthermore, the newly proposed synthetic procedure presents a reduced number of steps compared to that previously reported [22], with consequent significant advantages in terms of time and costs.

Cy5 was chosen as the NIR fluorescent chromophore. It possesses promising spectroscopic properties, including narrow NIR absorption and emission bands, high molar extinction coefficient, high fluorescence quantum yield, long fluorescence lifetime, and excellent photostability. In addition, the Cy5 biological compatibility and minimal cytotoxicity, and, most importantly, the possibility to be synthesized by a straightforward and low-cost procedure, highlight this chromophore as a promising tool for biological applications [21,23].

Scheme 2 describes the synthesis of the fluorescent probe Vem-L-Cy5 **3**.

Compound **2** is firstly linked in a HATU-mediated amide coupling with 8-(Boc-amino)-3,6-dioxaoctanoic acid dicyclohexyl-amine salt in dry DMF, in the presence of DIPEA as base. Simple deprotection of the Boc group with trifluoroacetic acid in DCM and the following coupling with Cy5 acid **4**, using the uronium salt HBTU and DIPEA as base, afford the fluorescent Vem-L-Cy5 **3**, finally purified by flash-chromatography. The synthesis of the fluorophore Cy5 acid **4** was performed as reported in literature [24].

2.2. Spectroscopic properties of Vem-L-Cy5 3

Absorption and fluorescence intensity analyses were conducted to investigate the spectroscopic properties of the synthesized probe **3** and how the absorption and emission spectra might be affected by the chemical environment. Specifically, Vem-L-Cy5 **3** was dissolved in DMSO, and the solution was diluted to a final concentration of 10 μM in

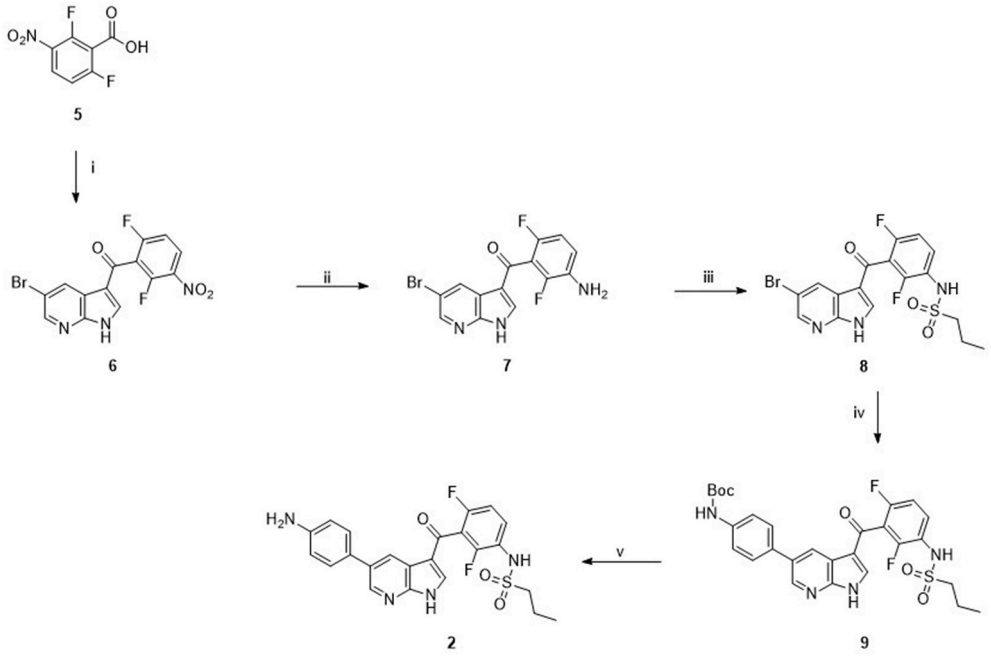

Scheme 1. Reagents and conditions: (i) a) dry DCM, dry DMF, oxalyl chloride, room temperature, overnight; b) $AlCl_3$, 5-bromo-7-azaindole, DCE, 50 °C, overnight, 92%; (ii) conc. HCI, Fe, EtOH, THF, 75 °C, 3 h, 86%; (iii) dry DCM, 1-propanesulfonylchloride, pyridine, room temperature, overnight, 89%; (iv) MeCN, 4-(*N*-Boc-amino)phenylboronic acid, $Pd(dppf)Cl_2$, 2 M Na_2CO_3, MW, 160 °C, 30 min, 71%; (v) dry DCM, TFA, room temperature, 3 h, 98%.

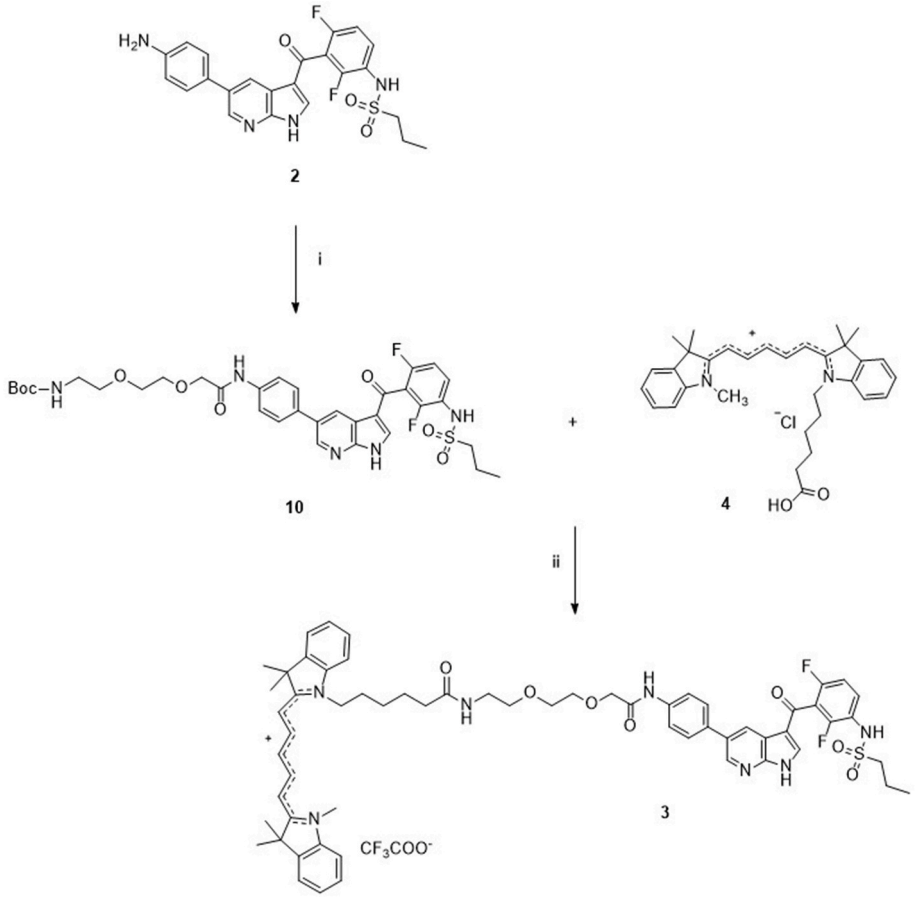

Scheme 2. Reagents and conditions: (i) dry DMF, 8-(Boc-amino)-3,6-dioxa-octanoic acid-DCA salt, HATU, DIPEA, room temperature, overnight, 81%; (ii) a) DCM, TFA, room temperature, 2 h, b) dry DMF, HBTU, DIPEA, room temperature, overnight, 49%.

different assay solutions (from aqueous to 60% v/v dioxane-water phosphate-buffered saline (PBS)). The percentage of DMSO did not exceed 1% of the final assay volume solution.

Fig. 1 shows the absorption spectra of **3**. In aqueous solution, the absorption spectrum shows a wide curve flattened on the abscissa axis. When **3** is dissolved in the PBS solution containing 20% of dioxane, the wavelength of maxima absorption is 645 nm with extinction coefficient ε of 12500 M^{-1} cm^{-1}. When the percentage of dioxane is increased to 40–60%, the wavelength of the absorption maxima remained nearly unchanged, but the spectra are characterized by an increase in the extinction coefficient.

Fig. 2 shows the emission spectra of Vem-L-Cy5 **3** at a 10 μM concentration. As expected, classic nonpolar solvatochromism was observed; indeed, a decrease in polarity of the environment (from aqueous to 60% dioxane in PBS) induces an increase of fluorescence emission intensity, while PBS only solution shows virtually no fluorescence intensity compared to the other three cases. The maximum wavelength of emission is in the range 655–665 nm for all the assay solutions. The same trends are also observed when the emission properties of Vem-L-Cy5 **3** are investigated at 5 μM and 1 μM concentrations (data not shown).

Experiments at three different concentrations were conducted to calculate the quantum yield (Φ) of Vem-L-Cy5 **3**. The data elaboration is referred to a standard solution of Cresyl Violet dissolved in MeOH and recorded at the same three concentrations of the samples. Results evidence that the quantum yield increases with increasing solvent lipophilicity (Table 1).

All in all, the spectroscopic properties of Vem-L-Cy5 **3** suggest a reduced background fluorescence from the non-bound fluorescent tracer, thus highlighting Vem-L-Cy5 **3** as a sound and valuable tool for further imaging applications.

2.3. Evaluation of Vem-L-Cy5 3 concentration and assessment of its stability

Fig. 3 shows the absorbance spectra of Cy5 **4** and Vem **1** at different concentrations, proving that the contribution of **1** at the wavelength of interest for the fluorochrome (640–660 nm) can be neglected. HPLC-UV analysis confirmed Cy5 **4** as the only absorber at 640–660 nm (Fig. S1, Supporting Information section). The calculation of the concentrations of Vem-L-Cy5 **3** was hence performed by spectrophotometric measurements at 640 nm, referring to a calibration curve composed of six known concentrations of Cy5 **4** (10/5/2.5/1.25/0.625/0.3125 μM). This is in fact a concentration range where Cy5 **4** and Vem-L-Cy5 **3** show a good linearity of both absorbance and fluorescence (Fig. S2, Supporting Information section).

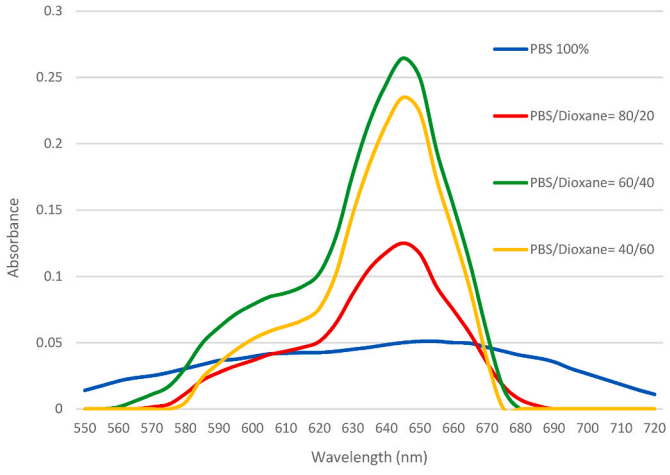

Fig. 1. Absorption spectra of **3** (10 μM) in solution varying from aqueous to 60% dioxane-PBS (v/v).

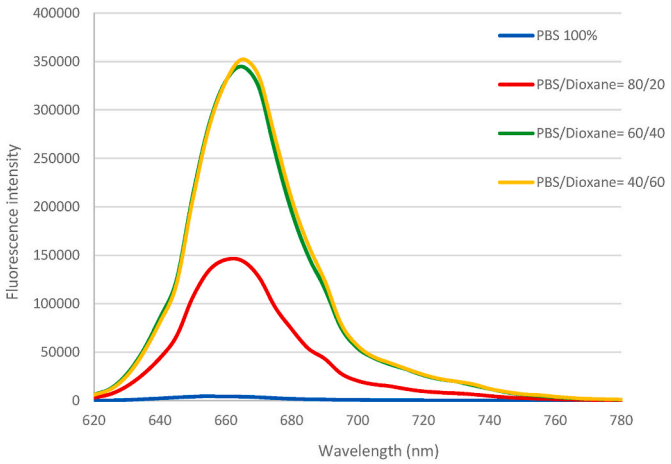

Fig. 2. Emission spectra of **3** (10 μM) in solution varying from aqueous to 60% dioxane-PBS (v/v).

Table 1
Quantum yield (Φ) of Vem-L-Cy5 **3** (referred to Cresyl Violet as standard) in solutions varying from aqueous to 60% dioxane–PBS.

Solution	Φ
PBS	0.0064
PBS/Dioxane 80/20	0.1493
PBS/Dioxane 60/40	0.2375
PBS/Dioxane 40/60	0.2725

The stability of Vem-L-Cy5 **3** was evaluated over time (2–48 h) at 37 °C in cell culture medium at pH 7.4, 5 and 8, as well as in serum (Foetal Bovine Serum, FBS). The chromatographic profile of Vem-L-Cy5 **3** remained unaltered in cell culture medium at neutral and alkaline pH, as well as in FBS (panels a, c, and d, Fig. S3, Supporting Information section). On the contrary, a modification in the profile was observed under acidic pH conditions. A splitting of peaks at 640 nm was recorded (panel b in Fig. S3, Supporting Information section). Furthermore, the absorbance of the dye at its wavelength maximum decreases over time, with a consequent decrease in the ratio of the peak area recorded at 640 and 330 nm (Fig. S4, Supporting Information section). This result is consistent with an instability of the dye at low pH. Indeed, discoloration of Vem-L-Cy5 **3** (from blue to almost colourless) was observed as well.

2.4. Biological properties of Vem-L-Cy5 3 in vitro

The biological investigation had the purpose to determine whether Vem-L-Cy5 **3** displays a pharmacological profile like that of native Vem **1**. It was performed using $BRAF^{V600E}$ cancer cell lines derived from three representative solid tumors: 8505C anaplastic thyroid cancer (ATC) cell line (homozygous for $BRAF^{V600E}$ mutation); A375 (homozygous for $BRAF^{V600E}$ mutation), C32, and WM278 (heterozygous for $BRAF^{V600E}$ mutation) melanoma cell lines; HT29 colorectal cancer cell line (heterozygous for $BRAF^{V600E}$ mutation). At present, reliable HCL cell lines profiled for $BRAF^{V600E}$ mutation, representative of this malignancy, are not commercially available [25,26].

First, we tested whether Vem-L-Cy5 **3** penetrates inside cancer cells, is retained, and specifically binds to $BRAF^{V600E}$, which is its elective target. Indeed, in A375 cells the fluorescent Vem-L-Cy5 **3** was found to produce a bright and uniform signal, with minimal background noise (Fig. 4a). Furthermore, it should be observed that such a signal is mostly in the cytoplasm, which is the main subcellular localization of $BRAF^{V600E}$, hence it is consistent with specific binding. In fact, no cyan

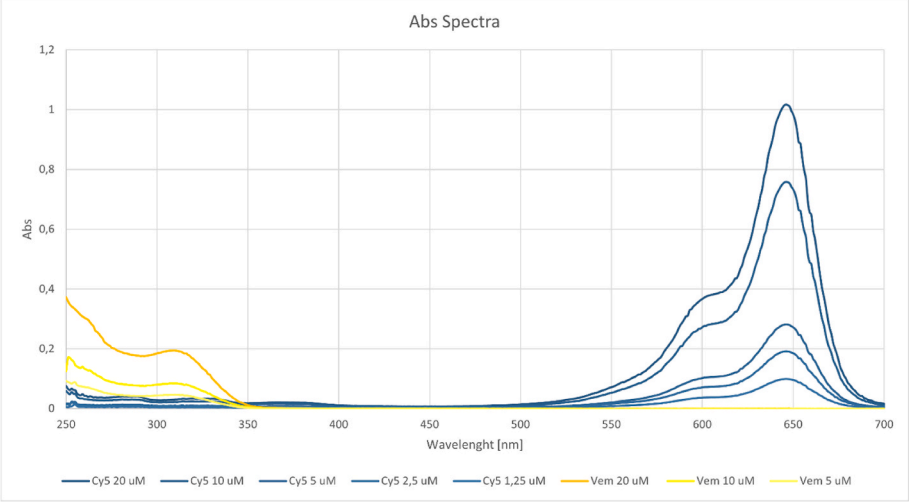

Fig. 3. Absorbance spectra of Vem **1** and Cy5 **4** showing the lack of contribution of Vem **1** at 640 nm and of Cy5 **4** at 320 nm.

fluorescence is evident in HeLa cells, a cervical cancer cell line that is wild type for BRAF and is used as negative control (Fig. 4b).

Once target specificity was established, we assessed whether the binding affinity of Vem-L-Cy5 **3** for $BRAF^{V600E}$ is similar to that of native Vem **1**. To this end, a displacement assay was performed: WM278 cells were pre-treated or not with a saturating concentration of Vem **1** (100 μM) for 30 min, and then treated with increasing concentrations of Vem-L-Cy5 **3** for additional 90 min. Cyan fluorescence was found to increase in a dose dependent manner, but the signal is lower in the case of pre-treatment with Vem **1** (Fig. 4c–d). This indicates that Vem-L-Cy5 **3** can displace the native drug **1** from its binding sites, hence it is endowed with similar binding affinity.

To further support these findings, the binding affinity of Vem-L-Cy5 **3** to $BRAF^{V600E}$ was evaluated by means of the KINOMEscan™ Kinase Binding Assay, according to manufacturer's protocol (see also Experimental section). We obtained that the K_d of Vem-L-Cy5 **3** is 13 nM (Fig. S5, Supporting Information section), which is very similar to the K_d 10 nM that is reported for Vem **1** [27] and attests the quality of our design strategy.

Finally, we tested whether Vem-L-Cy5 **3** maintains Vem **1** ability to inhibit MEK phosphorylation (Fig. 4e–f) and, consequently, cancer cell growth (Fig. 4g–j). Indeed, we found that this is the case in all four $BRAF^{V600E}$ cell lines tested, although we noticed that in three out of four cell lines the IC_{50} of Vem-L-Cy5 **3** is higher compared to the one of Vem **1** (A375, C32 and HT29, Fig. 4k). By comparing the cytotoxicity of Vem-L-Cy5 **3** to that of the mix Vem **1** + Cy5 **4**, as well as to that of Vem **1** and Cy5 **4** alone, we also ruled out that the fluorophore contributes to Vem-L-Cy5 **3** cytotoxicity: Cy5 **4** does not increase the cytotoxicity of Vem **1** and becomes cytotoxic *per se* only at high concentrations (Fig. S6, Supporting Information section).

Interestingly, we found that Vem-NH_2 **2**, the synthesis intermediate of **3**, displays a high binding affinity to $BRAF^{V600E}$: by KINOMEscan™ Kinase Binding Assay we obtained a K_d of 2.8 nM (Fig. S5, Supporting Information section), which is even lower than that reported for Vem **1** (10 nM) [27]. Consistently, Vem-NH_2 **2** fully retains Vem **1** ability to inhibit MEK phosphorylation (Fig. 4e–f) and is an even stronger inhibitor of cancer cell growth (Fig. 4g–k). Therefore, Vem-NH_2 **2** stands out even more as a valuable synthon to obtain additional versions of fluorescent Vem **1**.

All in all, these results highlight that the conjugation of Vem **1** basic structure with the Cy5 fluorophore does not compromise the biological properties of Vem **1**, including its permeability, binding preferences, and efficacy. Hence, Vem-L-Cy5 **3** is a useful tool to better understand the molecular mechanisms of Vem **1** activity.

2.5. Molecular modeling of Vem-L-Cy5 3 interaction with $BRAF^{V600E}$

To get deeper insights into the mode of action of **3**, molecular modeling studies were undertaken. To provide a viable three-dimensional (3D) model of the $BRAF^{V600E}$ complex at molecular level, the 3D X-ray structure of the $BRAF^{E}$ kinase domain in complex with a closed analogue of **1** was considered (PDB 5JRQ) [28]. In particular, the co-crystal ligand features a methoxy group in place of the chlorine at the *para* position of the pendant phenyl ring. At first, docking experiments of **3** (in both its two protomeric states, see experimental section) were attempted with Glide but no viable high scoring binding poses were produced for these calculations. This is likely due to the well-known limitations connected with docking experiments when trying to dock large and flexible ligands. Most precisely, search algorithms usually fail to converge toward a well-defined binding pose when dealing with many rotatable bonds (notably **3** features 25 rotatable bonds) and when a large portion of the compound is not expected to take direct contacts with the target protein. In this case, since linear scoring function tend to maximize ligand-receptor atom pair interactions, the presumably solvent exposed part would be forced to take direct contact with the protein rather than with the solvent, thereby leading to artifactual results.

Taking advantage of the experimental data outlining the competitive binding nature of **3** with **1** (see Fig. 4c–d above), the studied ligand was manually adapted in the $BRAF^{V600E}$ binding site to superimpose the Vem portion on that of the co-crystal ligand. On the other hand, the dye portion of **3** was allowed to project into the external region of the protein towards the solvent. This starting structure was subjected to a 500 ns long molecular dynamics (MD) simulation and results were analyzed by examining the ligand root mean square deviations and fluctuations (L-rmsd and L-rmsf, respectively) to profile the modifications in the ligand atom positions (Fig. 5).

Regardless of the considered protomeric state of **3**, as reported in Fig. 5b, the predicted binding mode is very stable throughout the entire production run. Analysis of the primary ligand fluctuations broken by atom demonstrates that the solvent-exposed region (i.e., the dye moiety) is the most flexible one, while the Vem part is adopting a stable conformation (Fig. 5b). As represented in Fig. 5c and d, the pyrrolopyridine ring forms two stable H-bonds (occurring for 99% of the simulations) with the backbone atoms of Gln530 and Cys532 hinge region residues. Additional and comparatively stable interactions are also established by the benzoyl moiety, which forms a water-bridged H-bond with Asp594, a cation-π interaction with Lys483 and additional H-bonds with Asp594 and its sulphonamide substituent. Lipophilic contacts are also engaged between the propyl groups and Leu514 sidechain. On the

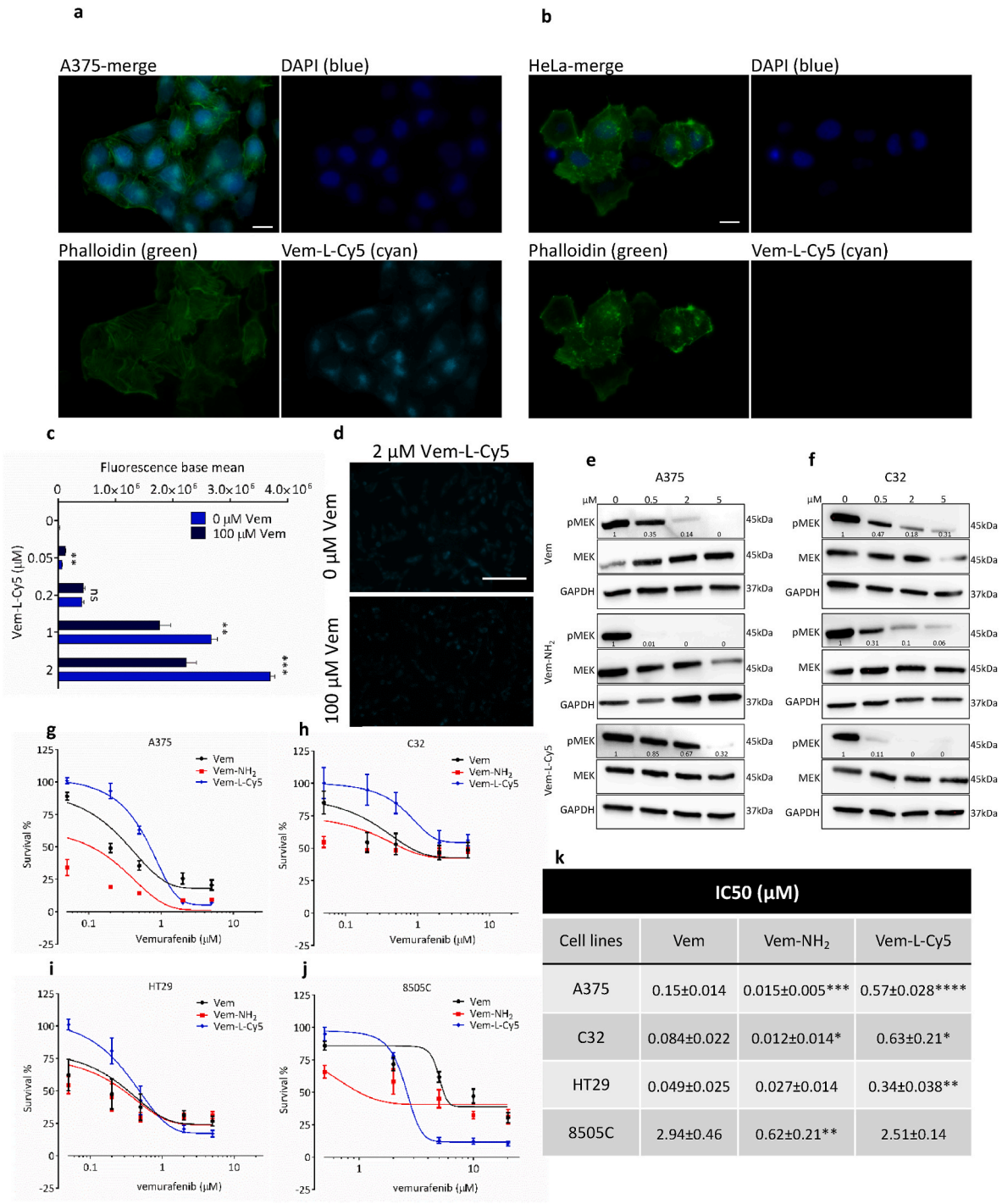

k

IC50 (µM)			
Cell lines	Vem	Vem-NH_2	Vem-L-Cy5
A375	0.15±0.014	0.015±0.005***	0.57±0.028****
C32	0.084±0.022	0.012±0.014*	0.63±0.21*
HT29	0.049±0.025	0.027±0.014	0.34±0.038**
8505C	2.94±0.46	0.62±0.21**	2.51±0.14

Fig. 4. Comparison of Vem **1** and Vem-L-Cy5 **3** as $BRAF^{V600E}$ inhibitors

(a-b) Penetration of Vem-L-Cy5 **3**, retention and specificity of binding to $BRAF^{V600E}$. A bright and uniform cyan fluorescence is evident only in the cytoplasm of A375 cells (carrying homozygous $BRAF^{V600E}$ mutation, a) and not in HeLa cells (wt for BRAF, b). Pictures were taken after 48 h of treatment with 0.5 µM drug concentration. Blue: DAPI; green: Phalloidin; cyan: Vem-L-Cy5 **3**. Scale bar: 10 µm. (c–d) Displacement assay between native Vem and Vem-L-Cy5 **3**. WM278 cells were treated or not with 100 µM Vem for 30′ and then with increasing concentrations of Vem-L-Cy5 for the next 90'. (c) At the end of the 120′ of cumulative treatment, absolute quantification of cyan fluorescence was performed by flow cytometry. Vem-L-Cy5 signal increases in a dose dependent manner (blue bars), but in the case of pretreatment with native Vem (dark blue bars) it does so to a lesser extent. (d) Representative images of WM278 cells that were treated with 0 µM Vem (upper) or 100 µM Vem (lower) for 30′ and then with 2 µM Vem-L-Cy5 for the next 90'. Cyan signal is stronger in case of no pre-treatment with Vem. Scale bar: 50 µm. (e–f) Representative Western blot analysis of pMEK levels in A375 (e) and C32 (f) cells, after 1 h of treatment with increasing concentrations of Vem, Vem-NH_2 or Vem-L-Cy5. The quantification of pMEK/MEK ratio (fold change over no treatment (0 µM)) is reported. (g–j) Growth curve of A375 (g), C32 (h), HT29 (i), 8505C (j) cells that were treated for a week with increasing concentrations of Vem (black), Vem-NH_2 (red) or Vem-L-Cy5 (blue), in order to evaluate growth inhibition. 8505C ATC cells are intrinsically more resistant to Vem and were treated with a higher concentration range compared to the one routinely used on melanoma cell lines (PMID: 28445987; PMID: 30929607; PMID: 36765859; PMID: 37013641). (k) IC_{50} values of Vem, Vem-NH_2 and Vem-L-Cy5 in the same cell lines shown in (g–j). The graphs and table represent the mean ± SEM of at least 3 independent experiments. *p < 0.05, **p < 0.01, ***<0.001, ****<0.0001.

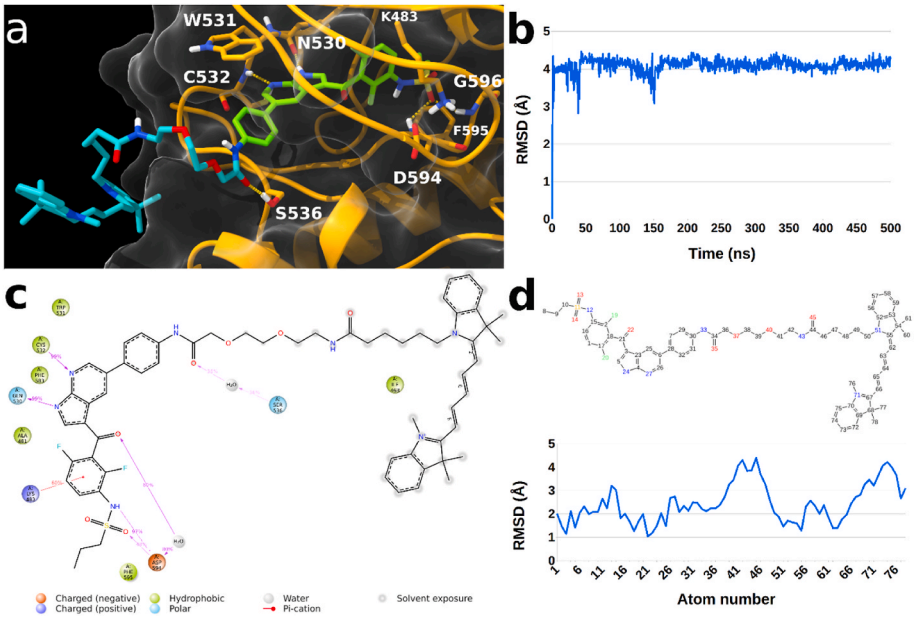

Fig. 5. Molecular modeling of Vem-L-Cy5 **3** interaction with $BRAF^{V600E}$.
(a) Energy-minimized representative frame of the 3D complex of **3**/$BRAF^{V600E}$ as calculated through MD simulations. The Vem and dye portions are represented as green and cyan sticks, respectively while the protein as orange sticks and ribbons and transparent surface. H-bonds are indicated by dashed yellow lines. (b) L-rmsd (Å) plot of **3** over time (ns). (c) Protein interactions of **3** throughout the simulation. (d) L-rmsf plot broken down by atom corresponding to the reported two-dimensional structure of **3**.

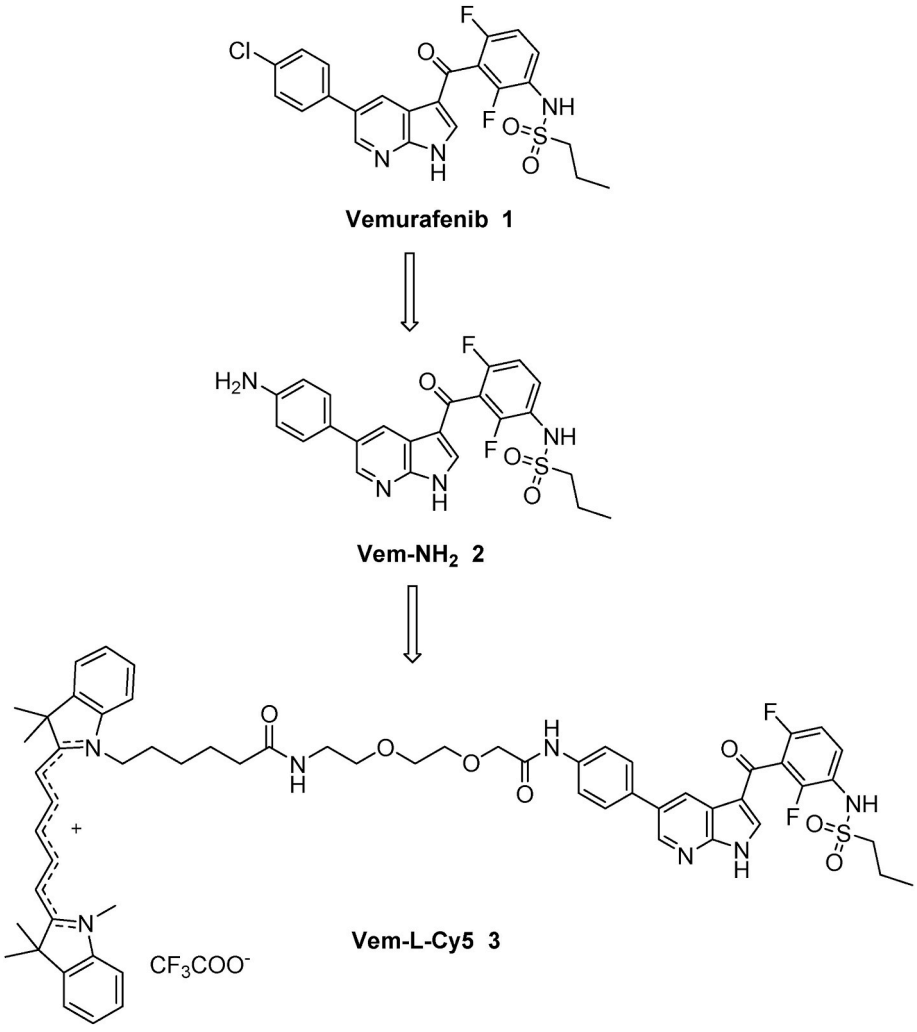

Chart 1. Conceptualization and structure of the fluorescent probe Vem-L-Cy5 **3.**

contrary, the PEG linker and the chromophore of **3** are exposed to the interaction with the solvent without establishing strong interactions with the protein. All in all, these data confirm the ability of **3** to establish the same interactions engaged by **1** with the $BRAF^{V600E}$ kinase domain. Interestingly, the linker and chromophore regions do not seem to negatively affect the binding to the protein thereby explaining why **3** features a similar affinity if compared to the precursor **2** which is devoid of the aforementioned groups.

3. Conclusions

A novel fluorescent imaging probe named Vem-L-Cy5 **3**, based on the structure of Vem **1**, was developed. The NIR Cy5 fluorophore combines the ability to avoid interfering autofluorescence of biomolecules with synthetic feasibility, high stability, biological compatibility, and promising spectroscopic properties. The experimental procedure for the obtainment of the key intermediate Vem-NH_2 **2**, which constitutes a versatile building block suitable for conjugation with different chromophores for specific imaging applications, was newly set up and optimized, resulting to be more straightforward and with lower cost compared to the one previously published by Mikula et al. [22].

Vem-L-Cy5 **3** was chemical-physical characterized by means of spectroscopic analyses, and biologically validated using cancer cell lines representative of three solid tumor types with $BRAF^{V600E}$ mutation (melanoma (A375, C32 and WM278 cell lines), colorectal cancer (HT29 cell line) and anaplastic thyroid carcinoma (8505C cell line)). These experiments allowed us to show that probe **3** penetrates inside cancer cells, specifically and efficiently binds to its elective target $BRAF^{V600E}$ and retains Vem **1** ability to inhibit MEK phosphorylation and cancer cell growth. Additionally, molecular modeling studies were attained to propose a viable model for the interaction of Vem-L-Cy5 **3** with $BRAF^{V600E}$.

In view of all these findings, Vem-L-Cy5 **3** has a great potential as fluorescent probe for applications in imaging studies aimed at a deeper investigation of Vem **1** molecular mechanisms, as well as in aiding the set up of valuable model cell lines for tumors in which $BRAF^{V600E}$ mutation is not fully profiled yet, including HCL. Information from these studies will be precious for the future discovery of new and safer small molecules allowing to effectively target $BRAF^{V600E}$-driven malignancies.

4. Experimental section

4.1. Chemistry

All reagents used were obtained from commercial source and all solvents were of an analytical grade. Anhydrous reactions were performed in flame-dried glassware under N_2. Rapid control on the progress of the reactions was carried out with analytical TLC on Merck 0.2 mm percolated silica gel aluminum sheets (60 F-254). Evaporation was performed in vacuum (rotary evaporator) and sometimes subsequentially drying was carried out with P_2O_5 as drying agent in vacuum desiccator. Compounds were purified through chromatography in column with silica gel (230–400 mesh ASTM) or in Isolera Biotage flash chromatography. Purity and chemical structure were checked with routine recordings of nuclear magnetic resonance spectra in DMSO-d_6 on a Bruker spectrometer operating at 400 MHz. Melting points were determined using Reichert Kofler hot-stage apparatus and are uncorrected. Absorption and fluorescence spectra were acquired by EnSight PerkinElmer. High-resolution ESI-MS spectra were performed on a Thermo LTQ Orbitrap XL mass spectrometer. Carbon, hydrogen, nitrogen and sulphur analyses were performed on a Vario MICRO cube instrument (Elementar).

2-[5-(1,3,3-Trimethyl-2,3-dihydro-1*H*-indol-2-ylidene)-1,3-pentadienyl]-3,3-dimethyl-1-(5-carboxypentyl)-3*H*-indolium chloride **4** has been prepared according to known procedure [24].

4.1.1. N-(3-(5-(4-Aminophenyl)-1H-pyrrolo[2,3-b]pyridine-3-carbonyl)-2,4-difluorophenyl)propane-1-sulfonamide (2)

To a solution of compound **9** (0.195 g, 0.34 mmol) in dry DCM (7.0 mL), TFA (3.40 mL) is added dropwise. The solution is stirred at room temperature for 3 h, then slowly poured into a mixture of saturated $NaHCO_3$ solution (2.6 mL) and 1 M NaOH (9.0 mL) and extracted with EtOAc. The combined organic layers are dried over Na_2SO_4 and concentrated under reduced pressure. The crude product does not need any further purification. Yellow solid; yield 98%; mp 205–207 °C. ^{1}H NMR (400 MHz, DMSO-d_6): δ = 12.89 (s, 1H), 9.78 (s, 1H), 8.59 (d, J = 2.4 Hz, 1H), 8.48 (bs, 1H), 8.16 (s, 1H), 7.59–7.41 (m, 3H), 7.31–7.29 (m, 1H), 6.70 (d, 2H, J = 4.6 Hz), 5.30 (bs, 2H), 3.13 (t, J = 7.6 Hz, 2H), 1.77–1.71 (m, 2H), 0.97 (t, J = 7.4 Hz, 3H). ^{13}C NMR (100 MHz, DMSO-d_6): δ = 180.99, 156.49 (dd, J_{CF} = 245.0, 6.0 Hz), 152.77 (dd, J_{CF} = 247.0, 8.5 Hz), 149.00, 148.52, 143.77, 138.76, 132.72, 129.19 (d, J_{CF} = 9.0 Hz), 128.09, 125.86, 125.63, 122.37 (dd, J_{CF} = 14.5, 3.5 Hz), 118.76 (t, J_{CF} = 23.5 Hz), 118.04, 115.98, 114.93, 112.79 (dd, J_{CF} = 22.0, 4.0 Hz), 53.89, 17.29, 13.07.

4.1.2. 2-((1E,3E)-5-((E)-1-(6-((2-(2-(2-((4-(3-(2,6-Difluoro-3-(propylsulfonamido)benzoyl)-1H-pyrrolo[2,3-b]pyridin-5-yl)phenyl)amino)-2-oxoethoxy)ethoxy)ethyl)amino)-6-oxohexyl)-3,3-dimethylindolin-2-ylidene)penta-1,3-dien-1-yl)-1,3,3-trimethyl-3H-indol-1-ium trifluoroacetate (3)

Compound **10** (0.040 g, 0.05 mmol) is dissolved in dry DCM (6.7 mL) and TFA (3.35 mL) is added. The mixture is stirred for 2 h at room temperature, concentrated, and triturated with Et_2O. The precipitated formed is filtered and then dissolved with 1 mL of dry DMF and **4** (0.035 g, 0.06 mmol), HBTU (0.023 g, 0.06 mmol) and DIPEA (0.05 mL, 0.25 mmol) are added sequentially. The resulting solution is stirred at room temperature overnight, concentrated and purified by flash chromatography using DCM/MeOH (0–10%). Blue solid; yield 49%; mp 116–118 °C. ^{1}H NMR (400 MHz, DMSO-d_6): δ = 12.98 (s, 1H), 9.81 (s, 1H), 9.78 (bs, 1H), 8.69 (d, J = 2.4 Hz, 1H), 8.62 (bs, 1H), 8.32–8.23 (m, 2H), 8.23 (s, 1H), 7.80 (t, J = 5.6 Hz, 1H), 7.79 (d, J = 8.4 Hz, 2H), 7.70 (d, J = 8.4 Hz, 2H), 7.62–7.59 (m, 3H), 7.41–7.36 (m, 4H), 7.29–7.23 (m, 2H), 6.80 (bs, 1H), 6.57–6.51 (m, 1H), 6.30–6.22 (m, 2H), 4.12 (s, 2H), 4.07 (t, J = 5.6 Hz, 2H), 3.70–3.68 (m, 2H), 3.62–3.58 (m, 2H), 3.59 (s, 3H), 3.44 (t, J = 6.0 Hz, 2H), 3.23–3.21 (m, 2H), 3.15–3.11 (m, 2H), 2.08 (t, J = 6.8 Hz, 2H), 1.75–1.67 (m, 2H), 1.67 (s, 6H), 1.54–1.53 (m, 2H), 1.38 (s, 6H), 1.36–1.34 (m, 2H), 1.27–1.15 (m, 2H), 0.97 (t, J = 7.0 Hz, 3H). ^{13}C NMR (100 MHz, DMSO-d_6): 182.11, 173.69, 172.98, 172.50, 168.83, 156.47 (dd, J_{CF} = 245.0, 7.0 Hz), 154.45, 152.82 (dd, J_{CF} = 246.0, 8.0 Hz),149.36, 143.98, 143.22, 142.45, 141.52, 141.45, 138.35, 133.79, 131.32, 129.18 (d, J_{CF} = 10.0 Hz), 128.86, 128.80, 127.76, 126.97, 125.83, 125.17, 125.08, 122.84, 122.73, 122.35 (dd, J_{CF} = 14.5, 4.0 Hz),120.65, 118.62 (t, J_{CF} = 24.0 Hz), 118.13, 116.28, 112.82 (dd, J_{CF} = 23.5, 4.0 Hz), 112.70, 111.48, 103.70, 103.50, 70.80, 70.74, 69.85, 69.65, 53.85, 49.30, 35.50, 31.52, 29.46, 27.62, 27.45, 27.14, 26.18, 25.32, 17.78, 13.37. HRMS (ESI) *m/z* Calculated for $C_{61}H_{68}F_2N_7O_7S^{+:}$ 1080.48635; Found: 1080.48547 [M^+]. Elementary analysis calculated for $C_{61}H_{68}F_2N_7O_7S \cdot 8H_2O \cdot CF_3COO^-$: C = 56.54; H = 6.33; N = 7.33; S = 2.40. Experimental: C = 56.16; H = 6.72; N = 7.07; S = 2.07.

4.1.3. (5-Bromo-1H-pyrrolo[2,3-b]pyridin3-yl)(2,6-difluoro-3-nitrophenyl)methanone (6)

To a solution of 2,6-difluoro-3-nitrobenzoic acid **5** (1.000 g, 5.00 mmol) in dry DMF (0.04 mL) and anhydrous DCM (10 mL), oxalyl chloride (1.890 g, 1.28 mL, 15.00 mmol) is added under nitrogen atmosphere. The resulting mixture is stirring overnight at room temperature. Solvents are then removed under vacuum to give the corresponding acyl chloride that is used in the following reaction without any further purification. To a solution of *5*-bromo-7-azaindole (0.986 g, 5.00 mmol) in DCE (15 mL) $AlCl_3$ (2.666 g, 20.00 mmol) is added portion wise at 0 °C under nitrogen atmosphere. Then, the acyl

chloride previously obtained is added and the resulting mixture is stirred at room temperature for 30 min and then heated at 50 °C overnight. After cooling, the solution is poured into ice and the solid precipitate formed is collected by vacuum filtration. The crude product does not need any further purification. Pale yellow solid; yield 92%; mp > 300 °C dec. ^{1}H NMR (400 MHz, DMSO-d_6): δ = 13.26 (s, 1H), 8.65 (d, J = 2.0 Hz, 1H), 8.54 (d, J = 2.0 Hz, 1H), 8.48–8.46 (m, 2H), 7.56 (t, J = 8.6 Hz, 1H). ^{13}C NMR (100 MHz, DMSO-d_6): δ = 179.39, 161.93 (dd, J_{CF} = 256.0, 7.0 Hz), 153.23 (dd, J_{CF} = 263.0, 9.0 Hz), 148.39, 145.99, 140.83, 134.79 (dd, J_{CF} = 7.5, 3.5 Hz), 131.71, 129.62 (d, J_{CF} = 10.0 Hz), 119.59 (t, J_{CF} = 24.0 Hz), 119.40, 115.14, 114.94, 113.80 (dd, J_{CF} = 24.0, 4.0 Hz).

4.1.4. (3-Amino-2,6-difluorophenyl)(5-bromo-1H-pyrrolo[2,3-b]pyridin-3-yl) methanone (7)

To a suspension of **6** (0.200 g, 0.52 mmol) in EtOH (2 mL) and THF (2 mL), concentrated HCl (0.52 mL) is added. After 10 min, Fe^0 (0.292 g, 5.20 mmol) is added, and the resulting mixture is heated to 75 °C for 3 h. After cooling, the mixture is filtered off and the precipitate washed with THF. The filtered solution is evaporated under vacuum. Then, water is added to the reaction flask and stirred for 1 h. The precipitate formed is filtered under vacuum. The product was finally purified by flash chromatography using EtOAc/petroleum ether 40–60 °C (5:5). Pale yellow solid; yield 86%; mp 255–257 °C. ^{1}H NMR (400 MHz, DMSO-d_6): δ = 13.05 (s, 1H), 8.56 (d, J = 4.0 Hz, 1H), 8.50 (d, J = 2.0 Hz, 1H), 8.16 (s, 1H), 6.98–6.87 (m, 2H), 5.23 (s, 2H). ^{13}C NMR (100 MHz, DMSO-d_6): δ = 182.69, 149.59 (dd, J_{CF} = 234.0, 6.0 Hz), 148.18, 146.41 (dd, J_{CF} = 241.0, 7.5 Hz), 145.55, 139.16, 133.92 (dd, J_{CF} = 13.0, 2.0 Hz), 119.55, 117.81 (d, J_{CF} = 20.0 Hz), 117.58 (d, J_{CF} = 20.0 Hz), 117.22 (t, J_{CF} = 8.0 Hz), 115.62, 114.57, 111.89 (dd, J_{CF} = 21.0, 3.0 Hz).

4.1.5. N-(3-(5-Bromo-1H-pyrrolo[2,3-b]pyridine-3-carbonyl)-2,4-difluorophenyl)propane-1-sulfonamide (8)

To a suspension of compound **7** (0.310 g, 0.88 mmol) in DCM (5.7 mL), pyridine (0.18 mL, 2.20 mmol) and 1-propanesulfonyl chloride (0.14 mL, 1.26 mmol) are added under nitrogen atmosphere. The mixture is stirred overnight at room temperature. The mixture is washed with water and then extracted with DCM, dried over Na_2SO_4, filtered, and evaporated to dryness. The crude product is finally purified by flash chromatography using EtOAc/petroleum ether 40–60 °C (6:4). White solid; yield 89%; mp 257–259 °C. ^{1}H NMR (400 MHz, DMSO-d_6): δ = 8.59 (s, 1H), 8.51 (d, J = 4.0 Hz, 1H), 8.29 (s, 1H), 7.62–7.56 (m, 1H), 7.30–7.26 (m, 1H), 3.13 (t, J = 7.8 Hz, 2H), 1.77–1.70 (m, 2H), 0.97 (t, J = 7.6 Hz, 3H). ^{13}C NMR (100 MHz, DMSO-d_6): δ = 181.13, 156.46 (dd, J_{CF} = 246.0, 6.5 Hz), 152.77 (dd, J_{CF} = 248.0, 9.0 Hz), 148.26, 145.77, 139.86 131.59, 129.44 (d, J_{CF} = 10.0 Hz), 122.41 (dd, J_{CF} = 14.0, 3.5 Hz), 119.49, 118.26 (t, J_{CF} = 24.0 Hz), 115.41, 114.75, 112.85 (dd, J_{CF} = 22.0, 3.5 Hz), 53.89, 17.29, 13.06.

4.1.6. Tert-butyl (4-(3-(2,6-difluoro-3-(propylsulfonamido)benzoyl)-1H-pyrrolo[2,3-b]pyridin-5-yl)phenyl)carbamate (9)

A solution of compound **8** (0.132 g, 0.29 mmol) and 4-(*N*-Boc-amino) phenylboronic acid (0.102 g, 0.44 mmol) in MeCN (1 mL) and 2 M aqueous solution of Na_2CO_3 (0.57 mL) is placed in a microwave vial. Pd (dppf)Cl_2 (0.024 g, 0.029 mmol) is added, and the mixture is irradiated in a microwave reactor (Biotage Initiator, Biotage, Uppsala, Sweden) at 160 °C for 30 min. The mixture is poured into water and extracted with EtOAc. The combined organic layers are dried over Na_2SO_4 and concentrated under reduced pressure. The crude product is finally purified by flash chromatography using EtOAc/petroleum ether 40–60 °C (4.5:5.5). Off-white solid; yield 71%; mp 230–232 °C. ^{1}H NMR (400 MHz, DMSO-d_6): δ = 12.96 (s, 1H), 9.78 (s, 1H), 9.51 (s, 1H), 8.67 (d, J = 2.0 Hz, 1H), 8.57 (bs, 1H), 8.22 (d, J = 2.2 Hz, 1H), 7.67–7.60 (m, 5H), 7.31–7.27 (m, 1H), 3.12 (t, J = 7.8 Hz, 2H), 1.78–1.71 (m, 2H), 1.51 (s, 9H), 0.96 (t, J = 7.4 Hz, 3H). ^{13}C NMR (100 MHz, DMSO-d_6): δ = 181.08, 156.48 (dd, J_{CF} = 245.0, 7.0 Hz), 153.23, 152.79 (dd, J_{CF} = 247.0, 8.5 Hz), 149.04, 144.22, 139.67, 132.11, 131.76, 129.17 (d, J_{CF} = 9.0 Hz), 127.80, 126.83, 122.40 (dd, J_{CF} = 13.0, 3.0 Hz), 119.11, 118.90 (t, J_{CF} = 24.0 Hz), 117.97, 116.07, 112.82 (dd, J_{CF} = 23.0, 4.0 Hz), 79.65, 53.89, 28.60, 17.29, 13.06.

4.1.7. Tert-butyl (2-(2-(2-((4-(3-(2,6-difluoro-3-(propylsulfonamido) benzoyl)-1H-pyrrolo[2,3-b]pyridin-5-yl)phenyl)amino)-2-oxoethoxy) ethoxy)ethyl)carbamate (10)

8-(Boc-amino)-3,6-dioxa-octanoic acid-DCA salt (0.172 g, 0.44 mmol), compound **2** (0.161 g, 0.34 mmol) and DIPEA (0.15 mL, 0.86 mmol) are dissolved in dry DMF (3 mL) and HATU (0.142 g, 0.37 mmol) is added. The reaction mixture is stirred at room temperature overnight, concentrated to ~1 mL and directly loaded onto a C18 column (Biotage, SFAR C18, 12 g). Reversed phase column chromatography using H_2O/MeCN (gradient elution, 3CV only H_2O, 1CV 1–6% MeCN, 20CV 6–50% MeCN, 5CV 50% MeCN, 10CV 50–60% MeCN) afforded the desired product **10**. Yellow solid; yield 81%; mp 162–164 °C. ^{1}H NMR (400 MHz, DMSO-d_6): δ = 9.77 (s, 1H), 8.70 (d, J = 2.0 Hz, 1H), 8.61 (bs, 1H), 8.21 (s, 1H), 7.81 (d, J = 8.8 Hz, 2H), 7.72 (d, J = 8.8 Hz, 2H), 7.61–7.55 (m, 1H), 7.27 (t, J = 8.0 Hz, 1H), 6.81 (t, J = 6.0 Hz, 1H), 4.13 (s, 2H), 3.70–3.69 (m, 2H), 3.63–3.61 (m, 2H), 3.46 (t, J = 6.0 Hz, 2H), 3.13–3.11 (m, 4H), 1.77–1.73 (m, 2H), 1.38 (s, 9H), 0.97 (t, J = 7.4 Hz, 3H). ^{13}C NMR (100 MHz, DMSO-d_6): δ = 181.12, 168.87, 156.41 (dd, J_{CF} = 243.0, 7.0 Hz), 156.10, 152.57 (dd, J_{CF} = 248.0, 8.0 Hz), 149.15, 144.27, 139.20, 138.43, 133.64, 131.60, 129.19 (d, J_{CF} = 10.0 Hz), 127.84, 127.02, 122.52 (dd, J_{CF} = 14.5, 3.5 Hz), 120.68, 118.63 (t, J_{CF} = 23.0 Hz), 117.98, 116.10, 112.80 (dd, J_{CF} = 22.5, 3.5 Hz), 78.08, 70.81, 70.71, 69.76, 69.72, 53.88, 28.68, 17.30, 13.07.

4.2. Determination of the fluorescence quantum yield

The quantum yield of the probe **3** (Φ_x) was determined according to equation:

$$\Phi_x = \Phi_{st}\left(\frac{D_x}{D_{st}}\right)\left(\frac{A_{st}}{A_x}\right)\left(\frac{\eta_x^2}{\eta_{st}^2}\right)$$

Where the subscript "st" and "x" denote respectively the standard and the test Vem-L-Cy5 **3**, Φ is the quantum yield, D is the area under the fluorescence emission spectra, A is the absorbance at the excitation wavelength, and η is the refractive index of the solvent or the mixture of solvents used. Cresyl violet (Φ = 0.54 in MeOH) is used as reference standard.

4.3. HPLC-UV analysis of Cy5 4, Vem 1, Vem 1 + Cy5 4, and Vem-L-Cy5 3 chromatograms, and of Vem-L-Cy5 3 stability over time in different conditions

Analyses were performed with reverse phase HPLC chromatography (Ultra-high-performance liquid chromatograph UltiMate® 3000, Dionex) on C18 column (Luna® 5 μm C8(2) 100 Å, LC Column 250 × 4.6 mm, Ea, part number 00G-4249-E0).

For chromatograms, solutions of Cy5 **4**, Vem **1**, Vem **1** + Cy5 **4**, and Vem-L-Cy5 **3** at a final concentration of 100 μM were prepared in a 1:1 mixture of DMSO-water. Elution was performed at 1 mL/min and a 30 min gradient was used: from 0 to 5 min 100% of 0.1% trifluoroacetic acid (TFA) in water; from 5 to 20 min, a linear gradient of 0.1% TFA in acetonitrile, ranging from 0 to 100%; from 20 to 21 min a linear gradient of 0.1% TFA in acetonitrile, ranging from 100% to 0%; from 21 to 30 min 100% of 0.1% TFA in water.

To test Vem-L-Cy5 stability, Vem-L-Cy5 **3** was incubated at 37 °C in DMEM High Glucose cell culture medium (without phenol red) at different pH (5, 7.4 and 8), or in Foetal Bovine Serum (FBS), for up to 48 h. The concentration in solution was 100 μM. At each time point, an aliquot was taken from the solution and analyzed. In the case of the serum solution, before the run, the serum was diluted 1:10 in cell culture

medium at pH 7.4. A 35 min gradient was used: from 0 to 1 min, 100% of 0.1% TFA in water; from 1 to 25 min, a linear gradient of 0.1% TFA in acetonitrile, ranging from 0 to 100%; from 25 to 26 min, a linear gradient of 0.1% TFA in acetonitrile, ranging from 100% to 0%; from 26 to 35 min, 100% of 0.1% TFA in water.

4.4. Evaluation of Vem-L-Cy5 3 concentration

In order to ensure that equimolar amounts of native Vem **1** and fluorescent Vem-L-Cy5 **3** are compared, the concentration of Vem-L-Cy5 **3** in the stock solution used for the administration to cell culture was estimated by absorbance measurement with Tecan Infinite M200 Pro plate reader, @ λ 640 nm. Specifically, after serial dilution, the concentration of Vem-L-Cy5 **3** was determined using a calibration curve composed of six known concentrations of Cy5 **4** 10/5/2.5/1.25/0.625/0.3125 μM.

4.5. Biological assays

4.5.1. Cell Culture

Cells were grown at 37 °C in a humidified atmosphere with 5% CO_2. 8505C anaplastic thyroid carcinoma cells (kind gift of Dr. F. Carlomagno, University of Naples, Italy) and A375 melanoma cells [29] were cultured in DMEM High Glucose supplemented with 10% Foetal Bovine Serum, 1% glutamine (Sigma-Aldrich) and 1% penicillin/streptomycin (Euroclone). C32 melanoma cells (Merck LifeScience) and HeLa cervical cancer cells [29] were cultured in MEM supplemented with 10% Foetal Bovine Serum, 1% glutamine (Sigma-Aldrich) and 1% penicillin/streptomycin (Euroclone). HT29 colorectal cancer cells [29] were cultured in McCoy's supplemented with 1% Foetal Bovine Serum, 1% glutamine (Sigma-Aldrich) and 1% penicillin/streptomycin (Euroclone). WM278 melanoma cells [29] were cultured in 4/5 MCDB 153 Media (Sigma-Aldrich), 1/5 Leibovitz L-15 Media (Euroclone), 2% Fetal Bovine Serum (Euroclone), 5 μg/μL Insulin (Sigma-Aldrich), 15 μg/μL Bovine Pituitary Extract (Millipore), 1.68 mmol/L CaCl2 (Sigma-Aldrich), 50 μg/mL Epidermal Growth Factor (BD Biosciences). Vemurafenib **1** (PLX-4032, S1267) was purchased from Selleckchem.

4.5.2. Detection of Vem-L-Cy5 3 by fluorescence microscopy

3×10^4 A375 and HeLa cells were seeded in 35/10 MM CellView Cell Culture Dish (Greiner Bio-One) and 24 h later they were treated with 0.5 μM Vem-L-Cy5 **3** or vehicle (DMSO). After 48 h, cells were washed with PBS and fixed with 4% formaldehyde for 10 min at room temperature. Then, they were stained with DAPI (4′,6-Diamidino-2-Phenylindole, Dihydrochloride, Invitrogen D1306) and Phalloidin (Phalloidin Cruz-Fluor™ 488 Conjugate, Santa Cruz sc-363791) diluted according to the manufacturer's instructions. Cells were visualized by fluorescence microscopy (Eclipse Ti2 Inverted Research microscope, Nikon).

4.5.3. Displacement assay

1.5×10^4 WM278 cells were seeded in 96-well plates and were grown for 24 h. On the day of imaging, cells were incubated with 0 or 100 μM concentrations of Vem **1** for 30 min at 37 °C. Without washing, fluorescent Vem-L-Cy5 **3** at different concentrations (0, 0.05, 0.2, 1 and 2 μM) was added for 90 more minutes. Then, cells were washed three times with media (15 min each) and live cells were imaged using Eclipse Ti2 Inverted Research microscope, Nikon. Then cells were detached to measure their fluorescence with flow cytometry (C6 Accuri, BD).

4.5.4. Growth curve assay with different doses of drug

Growth curve assays were carried out as previously described [30]. Briefly, 3×10^3 8505C cells and A375 cells, 10^4 C32 cells and 5×10^3 HT29 cells were seeded in 12 well plates and 24 h later they were treated with different doses of the appropriate drug or with vehicle (DMSO) for 7 days. Cells were then fixed with 4% PFA and stained with a crystal violet solution (0.1% crystal violet, 20% methanol, in water). After the excess crystal violet solution was removed and the plates were washed with tap water and dried, cells were de-stained using a 10% acetic acid solution. Absorbance was then read at 590 nm. Each sample was normalized on the vehicle-treated sample and the data were graphed as variation of cell percentage compared to the vehicle-treated sample.

4.5.5. Protein extraction and Western blot analysis

4×10^5 A375 and 7.5×10^5 C32 cells were seeded in p60 plates. 24 h later, they were treated with appropriate doses of drug or with vehicle (DMSO) for 1 h, and then harvested. As reported in literature [30], pellets were resuspended in 30 μl of lysis buffer (50 mM Tris HCl, 1% TritonX100, 0.25% NaDeoxicholate, 1 mM PMSF, 2 mM Orthovanadate, proteinase inhibitors cocktail). The mixture was incubated for 30 min on ice, then sonicated for 30 min and finally centrifuged at 14000 rpm for 30 min at 4 °C. The supernatant was then quantified using Bradford reagent and read at 590 nm. The samples were heated at 95 °C for 5 min, separated on 10% SDS-polyacrylamide gels (Mini-PROTEAN Precast gel, Bio-Rad) and electrotransferred to polyvinylidene difluoride (PVDF) membranes using Trans-Blot Turbo system (Bio-Rad). Membranes were blocked at room temperature for 2 h using 3% BSA in TBST for the detection of pMEK and of MEK or using 3% milk in TBST for the detection of GAPDH. They were then incubated overnight at 4 °C with the following primary antibodies: anti-Phospho-MEK 1/2 (#9154, Cell Signaling; rabbit polyclonal antibody, dilution 1:1000 in 3% BSA in TBST); anti-MEK 1/2 (#4694, Cell Signaling; mouse monoclonal antibody, dilution 1:1000 in 3% BSA in TBST); anti-GAPDH (#2118, Cell Signaling rabbit polyclonal antibody, dilution 1:3000 in 3% milk in TBST). According to the manufacturers' indications, all the primary antibodies used have been tested for their ability to recognize the relevant human proteins. The detection of primary antibodies was performed using alkaline phosphatase-conjugated secondary antibodies and enhanced chemiluminescence reagents (BIORAD, Clarity Western ECL Substrate).

4.5.6. Statistical analyses

Data were analyzed with unpaired *t*-test (GraphPad Prism, GraphPad Software Inc.). Values of $p < 0.05$ were considered statistically significant (*$p < 0.05$, **$p < 0.01$, ***$p < 0.001$, ****$p < 0.0001$). The mean ± SEM of three independent experiments is reported.

4.5.7. Kinase assay

Binding affinity of Vem-NH_2 **2** and Vem-L-Cy5 **3** to $BRAF^{V600E}$ was evaluated using the KINOMEscan™ Kinase Binding Assay (Eurofins, San Diego, CA), following the manufacturer's protocol. Briefly, KINOMEscan™ is based on a competition binding assay that quantitatively measures the ability of a compound to compete with an immobilized, active site-directed ligand. The assay is performed by combining three components: DNA-tagged kinase; immobilized ligand; and a test compound. The ability of the test compound to compete with the immobilized ligand is measured via quantitative PCR of the DNA tag. An 11-point 3-fold serial dilution of tested compound was prepared in 100% DMSO at 100x final test concentration, and subsequently diluted to 1x in the assay (final DMSO concentration = 1%). Kd was determined using a compound top concentration = 30 000 nM.

4.6. Molecular modeling

Docking calculations were attained employing the Glide tool implemented in Maestro [31]. The 3D structure of 3 in both its protomeric states (positive charge on one of the two heterocyclic nitrogens of the cyanine dye) were generated with the Maestro fragment Build tool and then energetically minimized with Macromodel [32]. The structure of $BRAF^{V600E}$ in complex with an methoxy analog of **1** (PDB code 5JRQ) [28] was downloaded from the Protein Data Bank and prepared through the Protein Preparation Wizard of the Maestro graphical user interface, which assigns bond orders, adds hydrogen atoms, and generates

appropriate protonation states. The docking grid box was centered on the co-crystal ligand with a grid box dimension equal to 30 Å × 30 Å × 30 Å. Finally, docking runs were carried out using the standard precision method.

MD simulations were run on the complex constructed as described above. This was used to build an MD simulation system. The complex was prepared using Maestro's system builder and solvated in an orthorhombic water box with a buffer distance of 10 Å. [33]. The system was neutralized with 8 Cl^-. The salt concentration was set to 0.15 M NaCl. The OPLS3 force field was used for the constructed receptor/ligand/membrane system [34].

The equilibration of the system was performed using NPT ensemble with default Desmond parameters (8-steps). The first 7-steps were considered as the short simulations known as the equilibration phase, as the temperature of the system is gradually increased, and the solute is restrained partially. The equilibrated system was then subjected to the 500ns MD final production along with PBC conditions and NPT ensemble. This simulation system was set up with 300 K temperature and 1atm pressure using the Martyna−Tobias−Klein barostat [35] and Nose−Hoover chain thermostat [36]. All pictures were rendered with the UCSF ChimeraX software [37].

Author contributions

The manuscript was written through contributions of all authors. All authors have given approval to the final version of the manuscript.

Declaration of competing interest

The authors declare that they have no known competing financial interests or personal relationships that could have appeared to influence the work reported in this paper.

Data availability

No data was used for the research described in the article.

Acknowledgments

This study was supported by AIRC [IG 2021 #25694]. It was also supported by ISPRO-Istituto per lo Studio, la Prevenzione e la Rete Oncologica [institutional funding]. The authors thank CISUP for the access to Thermo LTQ Orbitrap XL mass spectrometer laboratory facility.

Appendix A. Supplementary data

Supplementary data to this article can be found online at https://doi.org/10.1016/j.ejmech.2023.115446.

References

[1] Y.T. Lee, Y.J. Tan, C.E. Oon, Molecular targeted therapy: treating cancer with specificity, Eur. J. Pharmacol. 834 (2018) 188–196, https://doi.org/10.1016/J.EJPHAR.2018.07.034.
[2] V.V. Padma, An overview of targeted cancer therapy, Biomedicine 5 (4) (2015) 1–6, https://doi.org/10.7603/S40681-015-0019-4.
[3] B. Vogelstein, N. Papadopoulos, V.E. Velculescu, S. Zhou, L.A. Diaz, K.W. Kinzler, Cancer genome landscapes, Science 339 (6127) (2013) 1546–1558, https://doi.org/10.1126/SCIENCE.1235122E.
[4] A.M. Tsimberidou, E. Fountzilas, M. Nikanjam, R. Kurzrock, Review of precision cancer medicine: evolution of the treatment paradigm, Cancer Treat Rev. 86 (2020), 102019, https://doi.org/10.1016/J.CTRV.2020.102019.
[5] Z. Du, C.M. Lovly, Mechanisms of receptor tyrosine kinase activation in cancer, Mol. Cancer 17 (58) (2018), https://doi.org/10.1186/s12943-018-0782-4.
[6] T. Yamaoka, S. Kusumoto, K. Ando, M. Ohba, T. Ohmori, Receptor tyrosine kinase-targeted cancer therapy, Int. J. Mol. Sci. 19 (11) (2018) 3491, https://doi.org/10.3390/IJMS19113491.
[7] H. Davies, G.R. Bignell, C. Cox, P. Stephens, S. Edkins, S. Clegg, J. Teague, H. Woffendin, M.J. Garnett, W. Bottomley, N. Davis, E. Dicks, R. Ewing, Y. Floyd, K. Gray, S. Hall, R. Hawes, J. Hughes, V. Kosmidou, A. Menzies, C. Mould, A. Parker, C. Stevens, S. Watt, S. Hooper, H. Jayatilake, B.A. Gusterson, C. Cooper, J. Shipley, D. Hargrave, K. Pritchard-Jones, N. Maitland, G. Chenevix-Trench, G. J. Riggins, D.D. Bigner, G. Palmieri, A. Cossu, A. Flanagan, A. Nicholson, J.W. C. Ho, S.Y. Leung, S.T. Yuen, B.L. Weber, H.F. Seigler, T.L. Darrow, H. Paterson, R. Wooster, M.R. Stratton, P.A. Futreal, Mutations of the BRAF gene in human cancer, Nat 417 (6892) (2002) 949–954, https://doi.org/10.1038/nature00766.
[8] E. Tiacci, V. Trifonov, G. Schiavoni, A. Holmes, W. Kern, M.P. Martelli, A. Pucciarini, B. Bigerna, R. Pacini, V.A. Wells, P. Sportoletti, V. Pettirossi, R. Mannucci, O. Elliott, A. Liso, A. Ambrosetti, A. Pulsoni, F. Forconi, L. Trentin, G. Semenzato, G. Inghirami, M. Capponi, F. Di Raimondo, C. Patti, L. Arcaini, P. Musto, S. Pileri, C. Haferlach, S. Schnittger, G. Pizzolo, R. Foà, L. Farinelli, T. Haferlach, L. Pasqualucci, R. Rabadan, B. Falini, BRAF mutations in hairy-cell leukemia, N. Engl. J. Med. 364 (24) (2011) 2305–2315, https://doi.org/10.1056/NEJMoa1014209.
[9] A. Ahmadzadeh, S. Shahrabi, K. Jaseb, F. Norozi, M. Shahjahani, T. Vosoughi, S. Hajizamani, N. Saki, BRAF mutation in hairy cell leukemia, Onco Rev. 8 (2) (2014) 253, https://doi.org/10.4081/oncol.2014.253.
[10] P.A. Ascierto, J.M. Kirkwood, J.-J. Grob, E. Simeone, A.M. Grimaldi, M. Maio, G. Palmieri, A. Testori, F.M. Marincola, N. Mozzillo, The role of BRAF V600 mutation in melanoma, J. Transl. Med. 10 (2012) 85.
[11] G. Bollag, J. Tsai, J. Zhang, C. Zhang, P. Ibrahim, K. Nolop, P. Hirth, Vemurafenib: the first drug approved for BRAF-mutant cancer, Nat. Rev. Drug Discov. 11 (11) (2012) 873–886, https://doi.org/10.1038/nrd3847.
[12] S. Dietrich, J. Hüllein, M. Hundemer, N. Lehners, A. Jethwa, D. Capper, T. Acker, B. K. Garvalov, M. Andrulis, C. Blume, C. Schulte, T. Mandel, J. Meissner, S. Fröhling, C. Von Kalle, H. Glimm, A.D. Ho, T. Zenz, Continued response off treatment after BRAF inhibition in refractory hairy cell leukemia, J. Clin. Oncol. 31 (19) (2013), https://doi.org/10.1200/JCO.2012.45.9495.
[13] S. Dietrich, H. Glimm, M. Andrulis, C. von Kalle, A.D. Ho, T. Zenz, BRAF inhibition in refractory hairy-cell leukemia, N. Engl. J. Med. 366 (21) (2012) 2038–2040, https://doi.org/10.1056/nejmc1202124.
[14] F. Peyrade, D. Re, C. Ginet, L. Gastaud, M. Allegra, R. Ballotti, A. Thyss, T. Zenz, P. Auberger, G. Robert, Low-dose Vemurafenib induces complete remission in a case of hairy-cell leukemia with a V600E mutation, Haematologica 98 (2) (2013) e20–e22, https://doi.org/10.3324/haematol.2012.082404.
[15] G.A. Follows, H. Sims, D.M. Bloxham, T. Zenz, M.A. Hopper, H. Liu, A. Bench, P. Wright, M.B. van't Veer, M.A. Scott, Rapid response of biallelic BRAF V600E mutated hairy cell leukaemia to low dose Vemurafenib, Br. J. Haematol. 161 (1) (2013) 150–153, https://doi.org/10.1111/BJH.12201.
[16] P.B. Chapman, A. Hauschild, C. Robert, J.B. Haanen, P. Ascierto, J. Larkin, R. Dummer, C. Garbe, A. Testori, M. Maio, D. Hogg, P. Lorigan, C. Lebbe, T. Jouary, D. Schadendorf, A. Ribas, S.J. O'Day, J.A. Sosman, J.M. Kirkwood, A.M. M. Eggermont, B. Dreno, K. Nolop, J. Li, B. Nelson, J. Hou, R.J. Lee, K.T. Flaherty, G.A. McArthur, Improved survival with Vemurafenib in melanoma with BRAF V600E mutation, N. Engl. J. Med. 364 (26) (2011) 2507–2516, https://doi.org/10.1056/nejmoa1103782.
[17] A. Kim, M.S. Cohen, The discovery of Vemurafenib for the treatment of BRAF-mutated metastatic melanoma, Expet Opin. Drug Discov. 11 (9) (2016) 907–916, https://doi.org/10.1080/17460441.2016.1201057.
[18] V. Subbiah, C. Baik, J.M. Kirkwood, Clinical development of BRAF plus MEK inhibitor combinations, Trends in Cancer 6 (9) (2020) 797–810, https://doi.org/10.1016/J.TRECAN.2020.05.009.
[19] P. Queirolo, V. Picasso, F. Spagnolo, Combined BRAF and MEK inhibition for the treatment of BRAF-mutated metastatic melanoma, Cancer Treat Rev. 41 (6) (2015) 519–526, https://doi.org/10.1016/j.ctrv.2015.04.010.
[20] S.M. Usama, B. Zhao, K. Burgess, Fluorescent kinase inhibitors as probes in cancer, Chem. Soc. Rev. 50 (17) (2021) 9794–9816, https://doi.org/10.1039/D1CS00017A.
[21] J.O. Escobedo, O. Rusin, S. Lim, R.M. Strongin, NIR dyes for bioimaging applications, Curr. Opin. Chem. Biol. 14 (1) (2010) 64–70, https://doi.org/10.1016/J.CBPA.2009.10.022.
[22] H. Mikula, S. Stapleton, R.H. Kohler, C. Vinegoni, R. Weissleder, Design and development of fluorescent Vemurafenib analogs for in vivo imaging, Theranostics 7 (5) (2017) 1257–1265, https://doi.org/10.7150/thno.18238.
[23] P.C. Saha, T. Chatterjee, R. Pattanayak, R.S. Das, A. Mukherjee, M. Bhattacharyya, S. Guha, Targeting and imaging of mitochondria using near-infrared cyanine dye and its application to multicolor imaging, ACS Omega 4 (11) (2019) 14579–14588, https://doi.org/10.1021/acsomega.9b01890.
[24] M.V. Kvach, A.V. Ustinov, I.A. Stepanova, A.D. Malakhov, M.V. Skorobogatyi, V. V. Shmanai, V.A. Korshun, A convenient synthesis of cyanine dyes: reagents for the labeling of biomolecules, Eur. J. Org. Chem. 2008 (12) (2008) 2003–2174, https://doi.org/10.1002/EJOC.200701190.
[25] E. Tiacci, A. Pucciarini, B. Bigerna, V. Pettirossi, F. Strozzini, M.P. Martelli, A. Tabarrini, H.G. Drexler, B. Falini, Absence of BRAF-V600E in the human cell lines BONNA-12, ESKOL, HAIR-M, and HC-1 questions their origin from hairy cell leukemia, Blood 119 (22) (2012) 5332–5333, https://doi.org/10.1182/BLOOD-2011-12-400374.
[26] N.J. Weston-Bell, D. Hendriks, G. Sugiyarto, N.A. Bos, H.C. Kluin-Nelemans, F. Forconi, S.S. Sahota, Hairy cell leukemia cell lines expressing annexin A1 and displaying B-cell receptor signals characteristic of primary tumor cells lack the signature BRAF mutation to reveal unrepresentative origins, Leuk 27 (1) (2012) 241–245, https://doi.org/10.1038/leu.2012.163.
[27] G. Bollag, P. Hirth, J. Tsai, J. Zhang, P.N. Ibrahim, H. Cho, W. Spevak, C. Zhang, Y. Zhang, G. Habets, E.A. Burton, B. Wong, G. Tsang, B.L. West, B. Powell, R. Shellooe, A. Marimuthu, H. Nguyen, K.Y.J. Zhang, D.R. Artis, J. Schlessinger,

F. Su, B. Higgins, R. Iyer, K. Dandrea, A. Koehler, M. Stumm, P.S. Lin, R.J. Lee, J. Grippo, I. Puzanov, K.B. Kim, A. Ribas, G.A. McArthur, J.A. Sosman, P. B. Chapman, K.T. Flaherty, X. Xu, K.L. Nathanson, K. Nolop, Clinical efficacy of a RAF inhibitor needs broad target blockade in BRAF-mutant melanoma, Nature 467 (7315) (2010) 596–599, https://doi.org/10.1038/NATURE09454.

[28] M. Grasso, M.A. Estrada, C. Ventocilla, M. Samanta, J. Maksimoska, J. Villanueva, J.D. Winkler, R. Marmorstein, Chemically linked Vemurafenib inhibitors promote an inactive BRAFV600E conformation, ACS Chem. Biol. 11 (10) (2016) 2876–2888, https://doi.org/10.1021/acschembio.6B00529.

[29] A. Marranci, A. Tuccoli, M. Vitiello, E. Mercoledi, S. Sarti, S. Lubrano, M. Evangelista, A. Fogli, C. Valdes, F. Russo, M. Dal Monte, M.A. Caligo, M. Pellegrini, E. Capobianco, N. Tsinoremas, L. Poliseno, Identification of BRAF 3'UTR isoforms in melanoma, J. Invest. Dermatol. 135 (6) (2015) 1694–1697, https://doi.org/10.1038/JID.2015.47.

[30] M. Vitiello, M. Evangelista, Y. Zhang, L. Salmena, P.P. Pandolfi, L. Poliseno, PTENP1 is a CeRNA for PTEN: it's CRISPR clear, J. Hematol. Oncol. 13 (1) (2020) 1–5, https://doi.org/10.1186/S13045-020-00894-2.

[31] Schrödinger Release 2023-1: Maestro, Schrödinger, LLC, New York, NY, 2023.

[32] Schrödinger Release 2023-1, MacroModel;n Schrödinger, LLC, New York, NY, 2023.

[33] P. Mark, L. Nilsson, Structure and dynamics of the TIP3P, SPC, and SPC/E water models at 298 K, J. Phys. Chem. A 105 (43) (2001) 9954–9960, https://doi.org/10.1021/JP003020W.

[34] E. Harder, W. Damm, J. Maple, C. Wu, M. Reboul, J.Y. Xiang, L. Wang, D. Lupyan, M.K. Dahlgren, J.L. Knight, J.W. Kaus, D.S. Cerutti, G. Krilov, W.L. Jorgensen, R. Abel, R.A. Friesner, OPLS3: a force field providing broad coverage of drug-like small molecules and proteins, J. Chem. Theor. Comput. 12 (1) (2016) 281–296, https://doi.org/10.1021/ACS.JCTC.5B00864.

[35] G.J. Martyna, M.E. Tuckerman, D.J. Tobias, M.L. Klein, Explicit reversible integrators for extended systems dynamics, Mol. Phys. 87 (5) (1996) 1117–1157, https://doi.org/10.1080/00268979600100761.

[36] W.G. Hoover, Canonical dynamics: equilibrium phase-space distributions, Phys. Rev. A 31 (3) (1985) 1697, https://doi.org/10.1103/PhysRevA.31.1695.

[37] E.F. Pettersen, T.D. Goddard, C.C. Huang, G.S. Couch, D.M. Greenblatt, E.C. Meng, T.E. Ferrin, UCSF chimera - a visualization system for exploratory research and analysis, J. Comput. Chem. 25 (13) (2004) 1605–1612, https://doi.org/10.1002/jcc.20084.